Proceedings of the 6th International Conference on Gas Hydrates (ICGH 2008),
Vancouver, British Columbia, CANADA, July 6-10, 2008.

HYDROGEOCHEMICAL AND STRUCTURAL CONTROLS ON HETEROGENEOUS GAS HYDRATE DISTRIBUTION IN THE K-G BASIN OFFSHORE SE INDIA

Evan A. Solomon*
Scripps Institution of Oceanography
9500 Gilman Drive #0212, La Jolla, CA, 92093-0212
USA

Arthur J. Spivack
Graduate School of Oceanography
University of Rhode Island
Narragansett, RI 02882
USA

Miriam Kastner
Scripps Institution of Oceanography
9500 Gilman Drive #0212, La Jolla, CA, 92093-0212
USA

Marta Torres
College of Ocean and Atmospheric Sciences
Oregon State University
Corvallis, OR, 97331
USA

D.V. Borole
National Institute of Oceanography
Dona Paula 403 004, Goa
India

Gretchen Robertson
Scripps Institution of Oceanography
9500 Gilman Drive, La Jolla, CA, 92093
USA

Hamendra C. Das
Oil India Ltd.
Duliajan 786 602, Assam
India

* Corresponding author: Phone: +1 858 534 4857 Fax +1 858 822 4945 E-mail: esolomon@ucsd.edu

ABSTRACT

Natural gas hydrates occur on most continental margins in organic-rich sediments at water depths >450 m (in polar regions >150 m). Gas hydrate distribution and abundance, however, varies significantly from margin to margin and with tectonic environment. The National Gas Hydrate Program (NGHP) Expedition 01 cored 10 sites in the Krishna-Godawari (K-G) basin, located on the southeastern passive margin of India. The drilling at the K-G basin was comprehensive, providing an ideal location to address questions regarding processes that lead to variations in gas hydrate concentration and distribution in marine sediments. Pore fluids recovered from both pressurized and non-pressurized cores were analyzed for salinity, Cl^-, SO_4^{2-}, alkalinity, Ca^{2+}, Mg^{2+}, Sr^{2+}, Ba^{2+}, Na^+, and Li^+ concentrations, as well as δ^{13}C-DIC, δ^{18}O, and $^{87/86}$Sr isotope ratios. This comprehensive suite of pore fluid concentration and isotopic profiles places important constraints on the fluid/gas sources, transport pathways, and CH_4 fluxes, and their impact on gas hydrate concentration and distribution. Based on the Cl^- and δ^{18}O depth profiles, catwalk infrared images, pressure core CH_4 concentrations, and direct gas hydrate sampling, we show that the occurrence and concentration of gas hydrate varies considerably between sites. Gas hydrate was detected at all 10 sites, and occurs between 50 mbsf and the base of the gas hydrate stability zone (BGHSZ). In all but three sites cored, gas hydrate is mainly disseminated within the pore space with typical pore space occupancies being ≤2%. Massive occurrences of gas hydrate are controlled by high-angle fractures in clay/silt sediments at three sites, and locally by lithology (sand/silt) at the more "diffuse" sites with a maximum pore space occupancy of ~67%. Though a majority of the sites cored contained sand/silt horizons, little gas hydrate was observed in most of these intervals. At two sites in the K-G basin, we observe higher than seawater Cl^- concentrations between the sulfate-methane transition (SMT) and ~80 mbsf, suggesting active gas hydrate formation at rates faster than Cl^- diffusion and pore fluid advection. The fluids sampled within this depth range are chemically distinct from the fluids sampled below, and likely have been advected from a different source depth. These geochemical results provide the framework for a regional gas hydrate reservoir model that links the geology, geochemistry, and subsurface hydrology of the basin, with implications for the lateral heterogeneity of gas hydrate occurrence in continental margins.

Keywords: gas hydrates, fluid flow, pore fluid, NGHP

NOMENCLATURE

C_d Cl^- concentration after dissociation (mmol/m^3)
C_{pw} Background pore fluid Cl^- prior to dissociation (mmol/m^3)
V_h Volume fraction of gas hydrate filling pore space
C_h Cl^- concentration in gas hydrate (mmol/m^3)
ρ_{fw} density of freshwater (kg/m^3)
ρ_h density of gas hydrate (kg/m^3)
M_{fw} molecular weight of freshwater (g/mol)
M_h molecular weight of gas hydrate (g/mol)
m_{fw} moles of freshwater in 1 mole of gas hydrate
J diffusive flux of chemical constituent (mol/m^{2}yr)
D_o molecular diffusion coefficient (m^2/yr)
ϕ porosity
mbsf meters below seafloor
BGHSZ base of the gas hydrate stability zone
HSZ hydrate stability zone
BSR bottom simulating reflector
SMT sulfate-methane transition

INTRODUCTION

Gas hydrate distribution and abundance varies significantly in marine sediments. Gas hydrate occurrence in marine sediments typically occurs in two modes: (1) disseminated within fine-grained sediments at low concentrations or (2) massive along faults and fractures and within coarser-grained lithologies [1-4]. Most of the global marine gas hydrate reservoir is disseminated in sediments 100-300 m below the seafloor at water depths >450 m (in polar regions >150 m), and is often detected by associated free gas that produces a bottom simulating reflector (BSR) [5]. Massive occurrences of gas hydrate are often difficult to detect with traditional remote sensing methods (e.g. seismic surveys) as they are typically confined to relatively narrow fault and fracture

systems and associated with thin interbedded sand, silt, and volcanic ash layers. Massive gas hydrate deposits are often associated with high rates of

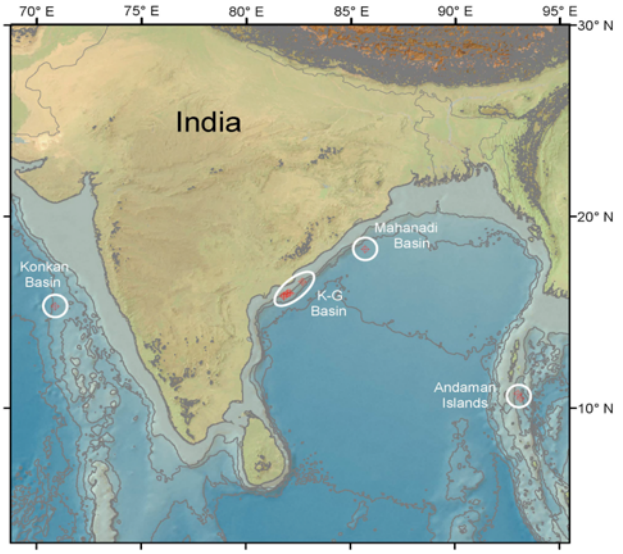

Figure 1| Location of K-G basin and other basins drilled during NGHP Expedition 01

fluid flow and hydrocarbon advection and occur close to the seafloor [6-7]. Evaluating the processes that lead to variations in gas hydrate distribution and concentration (disseminated versus massive) is crucial for guiding exploration and because gas hydrates form and persist within a stability field defined by gas solubility, pressure, and temperature [8-10], thus they are vulnerable to changes in sea level and bottom water temperature. These stability thresholds may be exceeded over geologic time destabilizing enormous quantities of gas hydrate, potentially triggering continental margin slope instability [11-12] and causing rapid climate change [13-14]. The estimated amount of methane carbon in marine gas hydrates ranges from ~$5{\cdot}10^{17}$ to 10^{19} g [15-16] and represents one of the largest reservoirs of methane on the planet. Thus, it is of critical importance to determine gas hydrates energy supply potential, as well as addressing questions pertaining to seafloor stability and environmental issues.

Legs 3 and 4 of the National Gas Hydrate Program (NGHP) Expedition 01 led by the Indian Directorate General of Hydrocarbons and the United States Geological Survey (USGS) cored ten sites exhibiting variable geologic conditions and BSR characteristics in the K-G basin in the Indian Ocean (Fig. 1) with the drillship *JOIDES Resolution* between June and August 2006. A logging while drilling (LWD) leg proceeded coring operations at the K-G basin sites, and three additional sites were drilled in the Mahanadi Basin and Andaman Sea during Leg 4 (Fig. 1). The objectives of the drilling campaign were to establish the structural and lithological controls on gas hydrate distribution and to asses the potential energy resource potential and environmental hazards offshore southeastern India. The drilling in the K-G basin was comprehensive (Fig. 2), and the high density of sites cored provides an ideal location to answer questions regarding processes that lead to variations in gas hydrate distribution and concentrations within marine sediments. For example, at three of the sites drilled (Sites 10, 12, and 21), massive gas hydrates were associated with heavily fractured clay-rich sediments (Fig. 3), whereas at the other sites gas hydrate was either massive within interbedded sand/silt layers or disseminated within clay-rich sediments. The close spacing between sites, the heterogeneous nature of gas hydrate occurrence within each of the sites, and the pronounced difference in gas hydrate distribution between adjacent sites provides an extraordinary natural laboratory and unique opportunity to address the following four questions: (1) What are the fluid and gas source(s), transport mechanisms, and 3-D migration pathways from source to reservoir? (2) What are the rates and quantities of CH_4 generated by local metabolic reactions in the cored sediments versus those delivered by advection from below the BGHSZ?

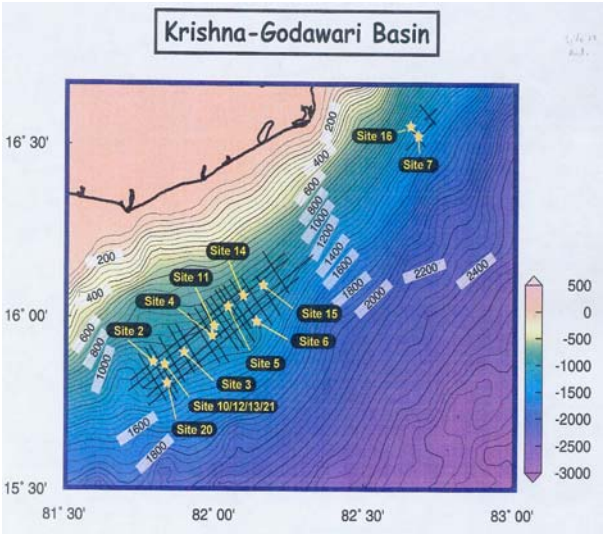

Figure 2| Bathymetric map showing locations of sites cored in the K-G basin [4]

(3) What is the depth, spatial distribution, and concentration of gas hydrates? (4) What are the geologic controls on the formation and occurrence of gas hydrates in the K-G basin?

To address these questions, a comprehensive suite of major, minor, and trace element concentrations, as well as isotope ratios were analyzed to deduce *in situ* diagenetic and metabolic reactions, fluids migrating from deeper within the sediment section, fluid and gas sources, fluid flow pathways, and the spatial distribution of gas hydrates.

Figure 3| Massive gas hydrate recovered from a core at Site 10. The gas hydrate is white and occurs along a high-angle fracture [4].

GEOLOGIC SETTING AND PORE FLUID SAMPLING STRATEGY

The eastern passive margin of India formed as a result of rifting between India and Australia/Antarctica in the Late Jurassic and Early Cretaceous. Sediment input into the Bay of Bengal is dominated by the Ganges-Brahmaputra river system, which drains much of the Himilayas. The sediment influx has built the Bengal Fan, which reaches a maximum sediment thickness of over 22 km on the Bangladesh shelf [17]. The sediment thickness at the location of the K-G basin drill sites is 8-10 km [4]. The sedimentation at the drill sites is dominated by river input and the organic matter in the sediments is mainly terrestrial in origin. The seismic lines in the K-G basin show features typical of fans including cut and filled channels and abundant growth faulting, and the sediments are primarily clays with well-defined silt/sand horizons [4]. High-resolution 2-D seismic lines in the vicinity of Sites 10&12 show a highly disrupted and faulted sedimentary sequence between the seafloor and ~150 mbsf. Individual reflectors, however, can only be traced a few hundred meters at most [4], and massive gas hydrates were recovered within this fault/fracture system.

During NGHP Expedition 01, 10 sites were cored in the K-G basin, and ~530 whole-round samples were collected at high-resolution ranging from 3-18 samples per 9 m of core for geochemical analyses. The highest resolution sampling was performed in the upper 40 m of the sediment column to characterize the SMT for future geochemical modeling studies and to provide supporting samples and data for studies on the microbial dynamics of the SMT. The LWD results guided the coring operations and whole-rounds were collected from both conventional cores and pressure cores. Whole-round sampling of conventional cores was guided by catwalk infrared scans, so that both background and gas hydrate-bearing sections were sampled. Pressure cores were sub-sampled for pore fluid geochemical analyses based on X-ray images of the cores taken before and after degassing, which placed constraints on the spatial distribution of the gas hydrate.

METHODS

Analytical

Whole-round samples collected for pore fluid analyses were carefully cleaned by removal of outside layers of sediment potentially contaminated by drilling fluid. The cleaned sediment samples were placed in titanium squeezers and the pore fluids were extracted at gauge forces ranging from 2,000 to 30,000 lbs. The pore fluids were then filtered through 0.45 μm Gelman polysulfone filters and immediately analyzed shipboard for salinity, Cl^-, alkalinity, sulfate, and Br^- concentrations. The remaining fluid was preserved for shore-based concentration and isotopic analyses. Salinity was analyzed by refractometry, Cl^- via titration with $AgNO_3$, and alkalinity by Gran titration. Sub-samples for sulfate analyses were added to centrifuge tubes containing a 50% $Cd(NO_3)_2$ solution to precipitate out the sulfide, and analyzed along with Br^- by ion chromatography. Shore-based Ca^{2+}, Mg^{2+}, Sr^{2+}, and Na^+ analyses were determined by inductively coupled plasma-optical emission spectrometry

(ICP-OES), and Li^+ and Ba^{2+} were determined by ICP-mass spectrometry (ICP-MS). The $\delta^{13}C$-DIC and $\delta^{18}O$ ratios were determined by stable isotope ratio mass spectrometry, and the $^{87/86}Sr$ isotope ratios via thermal ionization mass spectrometry (TIMS).

All shore-based samples, standards, and blanks were prepared in a clean laboratory. The reproducibility of the concentration analyses expressed as percent precision from multiple determinations of certified standards are: Cl = 0.2%, SO_4^{2-} = 0.5%, Br^- <1%, Ca^{2+} <1%, Mg^{2+} <1%, Sr^{2+} = 1%, Na^+ <3%, Ba^{2+} = 0.5%, and Li^+ = 1%. The standard deviations of the $^{87/86}Sr$, $\delta^{13}C$-DIC, and $\delta^{18}O$ analyses are ± 0.000020, ± 0.01‰, and ± 0.03‰, respectively.

General Calculations

When gas hydrate forms, water molecules are removed from the surrounding pore fluid excluding dissolved ions, thus increasing the pore fluid salinity and Cl^- concentrations. Gas hydrate dissociation causes freshening of the *in situ* pore fluid. Gas hydrate that is present in the sediment column prior to coring dissociates during the drilling and core retrieval process, releasing freshwater into the sediment pore space. The dilution of the pore fluid Cl^- concentrations provides an estimate of the amount of gas hydrate present prior to dissociation. To estimate gas hydrate abundance from Cl^- data requires knowledge of the *in situ* dissolved Cl^- concentration-depth profile prior to gas hydrate dissociation. The high frequency of pore fluid sampling on NGHP Expedition 01 in combination with the background whole-round sampling based on catwalk IR images and x-ray images from pressure core samples provides robust constraints on the background Cl^- values against which gas hydrate concentrations can be estimated. The Cl^- concentration after gas hydrate dissociation can be computed using the mixing equation presented in Ussler and Paull [18]:

$$C_d = C_{pw}[1-V_h/(w-(w-1)V_h)] + C_h[V_h/(w-(w-1)V_h)] \quad (1)$$

The variable w is computed from the following equation:

$$w = (\rho_{fw}M_h)/(\rho_h M_{fw} m_{fw}) \quad (2)$$

The primary objectives of the high-resolution sampling in the upper 40 m of sediments in the K-G basin was to characterize the SMT for geochemical modeling of methane fluxes. At the SMT, in some environments, microorganisms symbiotically reduce sulfate and oxidize methane by a process called anaerobic oxidation of methane (AOM). If AOM is complete, the stoichiometric ratio between the SO_4^{2-} and CH_4 consumed is 1:1, and the flux of sulfate to the SMT is equivalent to the upward methane flux to the SMT. The SMT depth varied from site to site in the K-G basin, and many of the densely sampled SO_4^{2-} profiles were linear. Based on the $\delta^{13}C$-DIC at these sites, it was determined which profiles were dominated by AOM, and the sulfate and CH_4 fluxes at these sites was computed by the following equation [19]:

$$J = \partial/\partial x[D_o\phi^3\partial C/\partial x] \quad (3)$$

The calculated sulfate flux is then assumed to be equivalent to the upward methane flux.

INITIAL RESULTS AND DISCUSSION

Chloride Concentrations and Gas Hydrate Distribution

Based on the dissolved Cl^- concentrations, $\delta^{18}O$ depth profiles, and catwalk infrared images, gas hydrate was present at all 10 sites cored. The occurrence and distribution of gas hydrate, however, varies considerably between the sites. The gas hydrate distribution in the K-G basin has been split into three groups: (1) disseminated gas hydrate within discrete intervals with low pore space occupancies (Sites 3, 7, 14, and 16; Fig. 4), (2) Sites with thick intervals of disseminated gas hydrate at moderate concentrations (Sites 5 and 20; Figs. 5B,D), and (3) Sites that contain massive gas hydrate associated with high-angle fractures in clay-dominated sediments or along coarser-grained sediment horizons (Sites 10, 15, 21; Fig. 5A, C).

The chloride concentration depth profiles at sites that have been binned in Group 1 are characterized by modern seawater concentrations (559 mM) from the seafloor to ~40 m above the BSR (approximately the depth of the BGHSZ; Fig. 4). The gas hydrate concentrations within this depth interval are typically ≤1% (pore space occupancy). At the Group 1 sites, near the BSR, there are isolated 10-20 m intervals with elevated

concentrations of gas hydrate that do not coincide with any changes in lithology manifested by minima in the Cl^- profiles ranging from 488-517 mM (Fig. 4). The minima in Cl^- concentrations in these 10-20 m zones indicate gas hydrate pore space occupancies ranging from 3-9%.

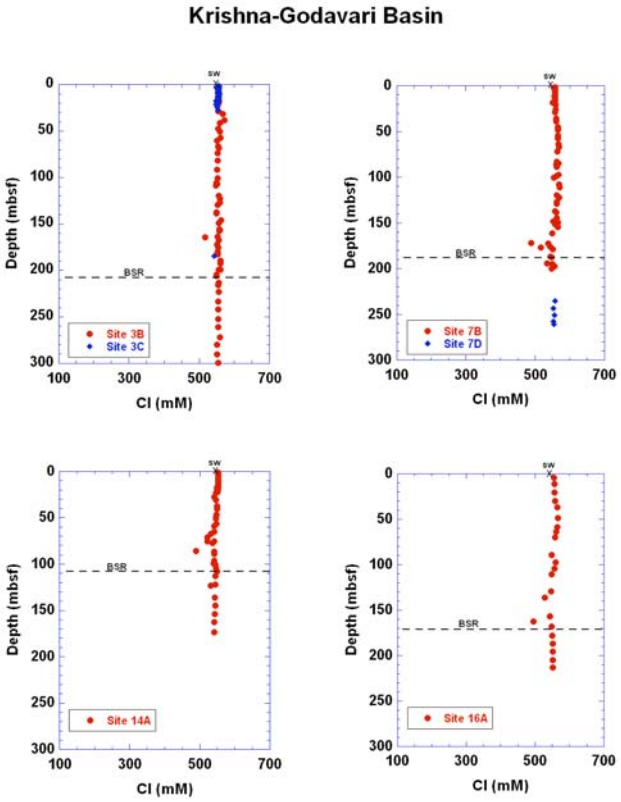

Figure 4| Cl^- concentration-depth profiles at sites containing disseminated gas hydrate within discrete intervals with low pore space occupancies. SW denotes seawater Cl^- concentration.

Sites that have been categorized as Group 2 sites also mainly contain gas hydrate that is disseminated in the sediment pore space, but the zone of gas hydrate occurrence is much thicker than the Group 1 sites (Fig. 5B,D). At these sites, disseminated gas hydrate, manifested by depleted pore fluid Cl^- concentrations relative to background values, was observed between ~50 mbsf and the BSR (Fig. 5B,D). At Site 5, gas hydrate concentrations increase towards the BSR and minima in the Cl^- concentration profile often coincide with coarser-grained lithologies (mainly interbedded silt). At both Sites 5 and 20, there is a ~60 m thick interval of sediments extending to the BSR harboring gas hydrate at pore space occupancies ranging from ~3-16%.

Sites 10,15, and 20 comprise Group 3, and are characterized by massive occurrences of gas hydrate. Sites 10 and 21 were drilled at the same location, and massive gas hydrate is associated with a high-angle fault and fracture system that extends from ~30 mbsf to the BSR (160 mbsf) at these sites. Chloride concentrations begin to decrease from modern seawater values at ~30 mbsf and reach a minimum value of 195 mM at ~80 mbsf (65% less than modern seawater value; Fig 5A, C), indicating a gas hydrate pore space occupancy of up to ~61% within this depth range. The thickness of the zone of massive gas hydrate occurrence at Sites 10 and 12 is ~130 m (Fig. 5A) with an average pore space occupancy of 30%. The background Cl^- concentration depth profile at Site 15 is characterized by chloride values that are only slightly depleted with respect to modern seawater (Fig. 5C) with gas hydrate concentrations ranging from 1-4% of the pore space volume. Superimposed on the background Cl^- concentrations is a sharp minimum in Cl^- values of 163 mM that is coincident with a sand layer. The gas hydrate-bearing sand contained an estimated gas hydrate pore volume occupancy of ~67%. During Expedition 01, we cored through numerous thick sand intervals similar to the one encountered at Site 15 that did not harbor significant quantities of gas hydrate. Understanding why some coarse-grained horizons harbor gas hydrate while others do not, even though they are within the hydrate stability zone, is currently being investigated and will provde valuable information for future gas hydrate drilling efforts.

Active Gas Hydrate Formation at Sites 5 and 10

At two sites in the K-G basin, we observe pore fluid Cl^- concentrations that are significantly elevated above modern seawater value (559 mM) over a vertical distance of 50-100 m below the SMT. At Site 5, chloride concentrations increase from 559 mM at 27 mbsf to 576 mM at 40 mbsf (~3% greater than seawater value; Fig. 5C). The Cl^- concentrations remain elevated to a depth of ~80 mbsf at Site 5. At Sites 10 and 21, background Cl^- concentrations increase above seawater value at ~15 mbsf and remain significantly higher than seawater concentration to ~130 mbsf with a concentration maximum of 663 mM at 80 mbsf (19% greater than seawater value; Fig. 5A). Minor increases in pore fluid salinity of

~2.5% have been observed in diffusive settings and attributed to increases in global ocean salinity during the last glacial maximum [20]. The extremely elevated Cl^- values at Sites 10 and 21 preclude trapped seawater as being the source of the elevated salinity observed below the SMT in the K-G basin sites, and the increase in pore fluid Cl^- is likely the result of gas hydrate formation within this interval.

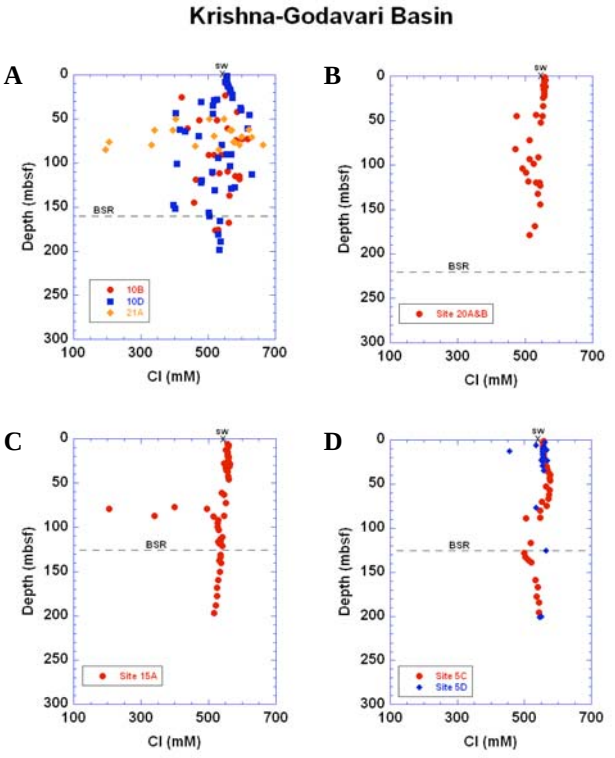

Figure 5| Cl^- concentration-depth profiles of (A,C) sites that contain massive gas hydrate and (B,D) sites with thick intervals of disseminated gas hydrate. SW denotes seawater Cl^- concentration.

Typically, the rate of *in situ* gas hydrate formation is slower than the rates of diffusion for the excluded ions. Thus, over time the salinity of the adjacent pore fluid does not greatly exceed the salinity of pore fluids above and below the zone of gas hydrate formation. Pore fluids with Cl^- concentrations of 809 mM in shallow sediments (1.2 mbsf) at southern Hydrate Ridge were attributed to elevated rates of gas hydrate formation driven by high fluid flow rates (45-300 cm/yr) and the presence of free gas in the advected fluids [21]. Coincident with the increase in Cl^- concentrations at Sites 5 and 10 is a depletion in pore fluid $\delta^{18}O$. The concomitant increase in Cl^- and depletion in $\delta^{18}O$ suggests active and sustained gas hydrate formation from the base of the SMT to 80 mbsf at Site 5 and to ~130 mbsf at Sites 10 and 21. Gas hydrate is likely forming at rates greater than ion diffusion and pore fluid advection. In order to sustain active gas hydrate formation over time requires a considerable and constant supply of CH_4 within the depth interval immediately below the SMT; a methane supply much greater than produced *in situ* [21]. Based on the pore fluid $^{87/86}Sr$ isotope ratios and minor element concentrations, the fluids sampled between the SMT and 80-130 mbsf is chemically distinct from those below this zone of active gas hydrate formation, suggesting they come from a different source region. Given that the fault/fracture system at Site 10 and the interbedded silt layers at Site 5 are more permeable than the surrounding clay-rich sediments, it is likey that these fluids originate at depths greater than the BGHSZ and that they are actively transporting CH_4 through permeable conduits to relatively shallow depths (<130 mbsf) driving gas hydrate precipitation.

VARIATIONS IN SMT DEPTHS AND ANAEROBIC OXIDATION OF METHANE

The primary objective of the high resolution sampling in the upper ~40 m of the sediment column at the K-G basin sites was to characterize the SMT for future geochemical modeling studies and to provide supporting data and samples for studies on the microbial dynamics of the SMT. Above the SMT, sulfate reducing microbial communities utilize interstitial SO_4^{2-} to oxidize organic matter by the following reaction:

$$2CH_2O + SO_4^{2-} \rightarrow 2HCO_3^- + H_2S + H_2O; \quad \delta^{13}C\text{-DIC} = 20\text{-}25‰ \qquad (4)$$

Below the transition zone, methanogens generate methane. At the interface where pore fluid SO_4^{2-} becomes depleted and CH_4 is produced, microorganisms symbiotically reduce sulfate and oxidize methane by a process called anaerobic oxidation of methane (AOM). AOM follows the net biogeochemical reaction:

$$CH_4 + SO_4^{2-} \rightarrow HCO_3^- + HS^- + H_2O; \quad \delta^{13}C\text{-DIC} < 30‰ \qquad (5)$$

When CH_4 oxidation by AOM is complete, usually in diffusional settings, but not necessarily in advection-dominated environments, all of the methane diffusing upwards is consumed before it enters the water column. It has conventionally been assumed that a steeper linear sulfate concentration gradient reflects higher CH_4 concentrations and rates of upward methane transport, and the sulfate gradients are modeled for CH_4 fluxes.

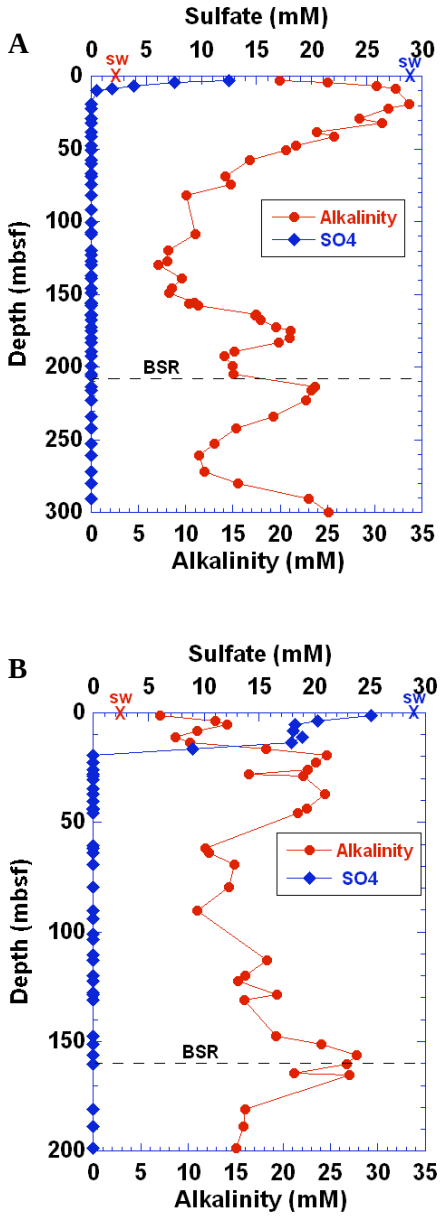

Figure 6| Sulfate and alkalinity concentration-depth profiles at (A) Site 3 and (B) Site 10.

The depth of the SMT varied between sites cored in the K-G basin ranging from 10 mbsf at Site 3 to 35 mbsf at Site 7. There is no consistent relationship between the depth of sulfate depletion and the occurrence of significant quantities of gas hydrate. For example, Site 3 contained the lowest overall gas hydrate concentrations, but has the shallowest SMT, whereas Site 10 has the highest gas hydrate occurrence associated with faults and fractures, but the SMT depth was relatively deep at ~20 mbsf (Fig. 6). These results contradict assumptions that a shallow SMT reflects high CH_4 fluxes, thus high subsurface gas hydrate concentrations. A massive occurrence of gas hydrate was also observed at Site 15, however this site has one of the deepest SMTs in the basin.

Sulfate reduction by AOM can be distinguished from SO_4^{2-} reduction by organic matter oxidation by the pore fluid δ^{13}C-DIC values and by the amount of alkalinity produced versus the amount of sulfate reduced. For every mole of SO_4^{2-} reduced during organic matter oxidation, 2 moles of HCO_3^- are produced, thus two moles of alkalinity are produced (Eq. 4). For every mole of SO_4^{2-} reduced during AOM, only one mole of alkalinity is produced (Eq. 5). In Figure 7, the change in alkalinity versus the change in sulfate from the seafloor to 10 m below the SMT is plotted for Sites 5, 10, and 20. The change in alkalinity has been corrected for Ca^{2+}, Mg^{2+}, and carbonate precipitation in authigenic carbonates. The blue line is the trajectory expected for SO_4^{2-} reduction by organic matter oxidation and the red line is that expected for AOM. As shown in Fig. 7, sulfate reduction by organic matter oxidation is the dominant biogeochemical process occurring in the upper 5 m of the sediment column, whereas both organic matter oxidation and AOM reduces sulfate from ~5 mbsf to the SMT.

The alkalinity production versus the sulfate reduction data coupled with the δ^{13}C-DIC values at the SMT indicate that nearly 2/3 of the sulfate profiles at the sites cored in the K-G basin are mainly controlled by organic matter oxidation, with only 1/3 dominated by AOM. These data indicate that the shallowest SMT at Site 3 is not the result of AOM, but is solely the result of organic matter oxidation. Sites 10 and 14 are the only sites where AOM is the dominant reaction controlling pore fluid SO_4^{2-} concnentrations, and the sulfate gradients have been used to estimate the upward diffusive flux of CH_4 at these sites by

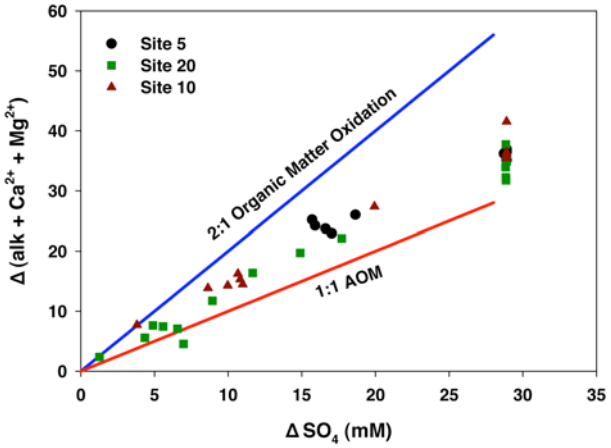

Figure 7| Plot of change in alkalinity (corrected for authigenic carbonate formation) versus change in sulfate from the seafloor to 10 m below the SMT at Sites 5, 10, and 20. The blue line is the expected values for oxidation of organic matter and the red line is the expected values for AOM.

Equation 3. The porosity and *in situ* temperature are tabulated in [4] and the molecular diffusion coefficient of SO_4^{2-} at the *in situ* temperature was calculated based on [22]. The sulfate gradient at Site 10 is 2.28 mM/m and at Site 14 it is 1.94 mM/m, and the downward diffusive SO_4^{2-} fluxes, thus upward CH_4 fluxes at Sites 10 and 14 are $1.4 \cdot 10^{-3}$ mmol/cm^{2}yr and $1.2 \cdot 10^{-3}$ mmol/cm^{2}yr, respectively. These are preliminary CH_4 flux estimates that do not account for the fraction of the pore fluid sulfate that is reduced by organic matter oxidation. More complete and robust estimates of the CH_4 fluxes at all of the sites in the K-G basin based on a new numerical biogeochemical model are in progress.

ACKNOWLEDGEMENTS

We thank the NGHP Expedition 01 shipboard scientific party for their assistance and thoughtful discussions during the expedition. We greatly appreciate the shipboard assistance and support of the staff and crew on-board the *JOIDES Resolution*. Funding for the project was provided by the Indian National Gas Hydrate Program, the Directorate General of Hydrocarbons under the Ministry of Petroleum and Natural Gas (India), and the US Department of Energy.

REFERENCES

[1] Paull, C.K., Matsumoto, R., Wallace, P.J., et al.. *Proc. ODP, Init. Repts.*, 164: College Station, TX (Ocean Drilling Program), 1996. doi:10.2973/odp.proc.ir.164.1996

[2] Tréhu, A.M, Bohrmann, G., Rack, F.R., Torres, M.E., et al. *Proc. ODP, Init. Repts.*, 204: College Station, TX (Ocean Drilling Program), 2003. doi:10.2973/odp.proc.ir.204.2003

[3] Riedel, M., Collett, T.S., Malone, M.J., and the Expedition 311 Scientists. *Proc. IODP*, 311: Washington, DC (Integrated Ocean Drilling Program Management International, Inc.), 2006. **doi:10.2204/iodp.proc.311.2006**

[4]] Collet, T., Riedel, M., Cochran, J., Boswell, R., Presley, J., Kumar, P., Sathe, A., Sethi, A., Lall, M., Siball, V., and the NGHP Expedition 01 Scientific Party. *Indian National Gas Hydrate Program Expedition 01 Initial Report*. Prepared by the U.S. Geological Survey and Published by the Directorate General of Hydrocarbons, Ministry of Petroleum & Natural Gas (India), 1DVD, 2008.

[5] Shipley, T.H., Houston, M.H., Buffler, R.T., Richard, T., Shaub, F.J., McMillen, K.J., Ladd, J.W., Worzel, J.L. *Seismic evidence for widespread possible gas hydrate horizons on continental slopes and rises*. Bull. Am. Assoc. Pet. Geol. 1979; 62: 2204-2213.

[6] Roberts, H.H., Carney, R. *Evidence of episodic fluid, gas, and sediment venting on the northern Gulf of Mexico slope*. Econ. Geol. 1997; 92: 863-879.

[7] Solomon, E.A., Kastner, M., Jannasch, H., Robertson, G., Weinstein, Y. *Dynamic fluid flow and chemical fluxes associated with a seafloor gas hydrate deposit on the northern Gulf of Mexico slope.* Earth and Planet. Sci. Lett 2008; in press.

[8]] Sloan, D.E. and Koh, C.A. *Clathrate hydrates of natural gases.* Boca Raton: CRC Press, 2008.

[9] Handa, Y.P. *Effect of hydrostatic pressure and salinity on the stability of gas hydrates*. J. Pys. Chem. 1990; 94: 2652-2657.

[10] Zatsepina, O.Y., Buffet, B.A. *Thermodynamic conditions for the study of gas hydrate in the seafloor*. J. Geophys. Res. 1998; 103: 24,127-24,139.

[11] Brewer, P.G. *Gas hydrates and global climatic change*, in: Gas Hydrates, Challenges for the Future, Annals, N.Y. Acad. Sci. 1999; 912: 195-199.

[12] Dillon, W.P., Danforth, W.W., Hutchinson, D.R., Drury, R.M., Taylor, M.H., Booth, J.S. Evidence for faulting related to dissociation of gas hydrate and release of methane from the southeastern United States, Gas Hydrates: Relevance to World Margin Stability and Climatic Change, in: Henriet, P.P., Mienert, J. (Eds.), Geol. Soc. Lond. Spec. Pub. 1998; 137: 293-302.
[13] Dickens, G.R., Castillo, M.M., Walker, J.C.G. *A blast of gas in the latest Paleocene: simulating first-order effects of massive dissocation of oceanic methane hydrate*. Geology 1997; 25: 259-262.
[14] Kennet, J.P., Cannariato, K.G., Hendy, I.L., Behl, R.J. *Carbon isotope evidence for methane hydrate instability during quaternary interstadials*. Science 2000; 288: 128-133.
[15] Kvenvolden, K.A. *Potential effects of gas hydrate on human welfare.* Proc. Nat. Ac. Sci. 1999; 96: 3420-3426.
[16] Milikov, A.V., Claypool, G.E., Lee, Y-J., Xu, W., Dickens, G.R., Borowski, W.S. *In situ methane concentrations at Hydrate Ridge, offshore Oregon: New constraints on the global gas hydrate inventory from an active margin*. Geology 2003; 31: 833-836.
[17] Curray, J.R. *Possible greenschist metemorphism at the base of a 22-km sedimentary section, Bay of Bengal.* Geology 1991; 19: 1097-1100.
[18] W. Ussler III, C.K. Paull. *Ion exclusion associated with marine gas hydrate deposits*, in: Natural Gas Hydrates: Occurrence, Distribution, and Detection, C.K. Paull and W.P. Dillon (eds.), American Geophysical Union, Geophysical Monograph 2001; 24: 41-65.
[19] W.S. Borowski, C.K. Paull, W. Ussler III. *Marine pore-water sulfate profiles indicate in situ methane flux from underlying gas hydrate*. Geology 1996; 24: 655-658.
[20] Adkins, J.F., Schrag, D.P. *Pore fluid constraints on deep ocean temperature and salinity during the last glacial maximum.* Geophys. Res. Lett. 2001; 28(5): doi:10.1029/2000GL011597.
[21] Haeckel, M., Suess, E., Wallman, K., Rickert, D. *Rising methane gas bubbles form massive hydrate layers at the seafloor*. Geochim. et Cosmochim. Acta 2004; 68(21): 4335-4345.
[22] Li, Y-H., Gregory, S. *Diffusion of ions in seawater and in deep-sea sediments*. Geochim. et Cosmochim. Acta 1974; 38: 703-714.